Published in final edited form as:

Clin Cancer Res. 2021 April 15; 27(8): 2266–2276. doi:10.1158/1078-0432.CCR-20-3882.

A novel mouse model of radiation-induced cardiac injury reveals biological and radiological biomarkers of cardiac dysfunction with potential clinical relevance

Alexandra D. Dreyfuss[1],

Denisa Goia[1],

Khayrullo Shoniyozov[1],

Swapnil V. Shewale[2],

Anastasia Velalopoulou[1],

Susan Mazzoni[1],

Harris Avgousti[1],

Scott D. Metzler[3],

Paco E. Bravo[3,4],

Steven J Feigenberg[1],

Bonnie Ky[4],

Ioannis I. Verginadis[*,1],

Constantinos Koumenis[*,1]

[1]Dept. of Radiation Oncology, University of Pennsylvania, Philadelphia, PA 19104

[2]Mouse Cardiovascular Phenotyping Core, Cardiovascular Institute, Dept. of Medicine, University of Pennsylvania, Philadelphia PA 19104

[3]Division of Nuclear Medicine, Dept. of Radiology, University of Pennsylvania, Philadelphia, PA 19104

[4]Division of Cardiology, Dept. of Medicine, University of Pennsylvania, Philadelphia, PA 19104

Abstract

Purpose: Radiation-induced cardiotoxicity is a significant concern in thoracic oncology patients. However, the basis for this disease pathology is not well-characterized. We developed a novel mouse model of radiation-induced cardiotoxicity to investigate pathophysiologic mechanisms and identify clinically targetable biomarkers of cardiac injury.

Corresponding authors: Ioannis Verginadis, University of Pennsylvania, Perelman School of Medicine, 3400 Civic Center Blvd., Bldg 421, Smilow Center for Translational Research, Room 8-160, Philadelphia, PA 19104-5156, vioannis@pennmedicine.upenn.edu; Constantinos Koumenis, University of Pennsylvania, Perelman School of Medicine, 3400 Civic Center Blvd., Bldg 421, Smilow Center for Translational Research, Room 8-124, Philadelphia, PA 19104-5156, Office: 215-898-0076, Fax: 215-898-0090, Lab: 215-898-0078, costas.koumenis@pennmedicine.upenn.edu.

*Co-senior authors

Conflicts of Interest: None

Experimental Design: Single radiation doses of 20, 40, or 60 Gy were delivered to the cardiac apex of female C57BL/6 mice aged 9–11 weeks, with or without adjacent lung tissue, using conformal radiation therapy (RT). Cardiac tissue was harvested up to 24 weeks post-RT for histologic analysis. Echocardiography and Technetium-99 sestamibi single photon emission computed tomography (SPECT) at 8 and 16 weeks post-RT were implemented to evaluate myocardial function and perfusion. Mouse cardiac tissue and mouse and human plasma were harvested for biochemical studies.

Results: Histopathologically, RT resulted in perivascular fibrosis 8 and 24 ($p<0.05$) weeks post-RT. Apical perfusion deficits on SPECT and systolic and diastolic dysfunction on echocardiography 8 and 16 weeks post-RT were also observed ($p<0.05$). Irradiated cardiac tissue and plasma showed significant increases in placental growth factor (PlGF), interleukin-6, and tumor necrosis factor-alpha (TNFα) compared to non-radiated matched controls, with greater increases in cardiac cytokine levels when RT involved lung. Human plasma showed increased PlGF ($p=0.021$) and TNFα ($p=0.036$) levels post-thoracic RT. PlGF levels demonstrated a strong correlation ($r=0.89$, $p=0.0001$) with mean heart dose.

Conclusions: We developed and characterized a pathophysiologically relevant mouse model of radiation-induced cardiotoxicity involving in situ irradiation of the cardiac apex. The model can be used to integrate radiomic and biochemical markers of cardiotoxicity to inform early therapeutic intervention and human translational studies.

Keywords

Radiation; cardiotoxicity; cardiac mouse model; fibrosis; PlGF; SPECT

INTRODUCTION

Radiation therapy (RT) has proven to be highly effective in controlling or eradicating solid tumors, with over half of all cancer patients expected to receive RT at some point in their disease course.[1] In the case of thoracic RT, a significant number of patients are at an increased risk of developing some form of cardiac disease due to incidental dose delivery to the heart.[2, 3, 4] As cardiovascular disease is now the most common non-malignant cause of death among cancer survivors,[5] there is a strong incentive to elucidate the causative pathophysiologic mechanisms of radiation-induced heart disease (RIHD).

RIHD is postulated to result from a series of events including direct DNA damage, increased oxidative stress, vascular endothelial cell injury, inflammation, and fibrosis.[6–9] However, our current understanding of such processes has been limited by a lack of physiologically relevant translational small animal models. Mezzaroma et al. described the use of a mouse model for the assessment of cardiomyopathy post-RT, however, the model requires irradiation of the entire thorax.[10] A more physiologically-relevant mouse model was reported by Seivert et al. involving irradiation of the entire heart and a portion of lung tissue.[11] However, whole heart irradiation is uncommon in clinical practice and also limits the ability to histologically and radiologically characterize the spatial patterning of RT-induced damage. We hypothesized that a more clinically relevant mouse model of RT-induced cardiotoxicity would be useful for investigating relevant pathophysiology and

could be generated by the irradiation of only a portion of the heart. The mouse model described in this study allows for targeted, in situ partial heart (PH) irradiation alone or with simultaneous partial lung (PHL) irradiation. Additionally, conformal RT was utilized to deliver high doses of RT with minimal skin toxicity and to better mimic RT administered in the clinic.

Despite extensive investigation, the role of sensitive imaging measures and biomarkers in signaling RT-induced cardiotoxicity has yet to be established. Early identification of radiomic and biochemical markers in thoracic RT patients with increased risk of cardiac complications would be useful in reducing treatment-associated morbidity and mortality through the implementation of more aggressive and targeted therapeutic interventions for RIHD. With respect to imaging, most clinical and preclinical data have relied on echocardiography to measure left ventricular ejection fraction (LVEF),[12] however, this approach fails to provide insight into the basis for mechanistic changes in cardiac function. With increasing evidence implicating vascular damage as an important mechanism of RT-induced cardiac injury,[13, 14] one radiomic approach is to implement Technetium-99 (Tc-99m) sestamibi single photon emission computed tomography (SPECT) to evaluate for myocardial perfusion defects. Additionally, from a biochemical perspective, several studies have demonstrated value in using circulating myocardial injury markers (troponin, pro brain natriuretic peptide), inflammatory markers (high sensitivity C reactive protein, growth differentiation factor, myeloperoxidase, cytokines) and vascular pathology markers (placental growth factor (PlGF)) to identify disease development following chemotherapy or RT in breast cancer, lung cancer, and lymphoma patients.[15, 16, 17, 18] Therefore, we used our model of RT-induced cardiotoxicity to evaluate radiologic and biochemical markers of cardiac injury, and leveraged our findings to guide subsequent human plasma biomarker identification studies. Our model is a valuable tool for understanding causative underlying pathophysiology and establishing predictive toxicity markers that signal the onset and progression of RIHD, before it becomes irreversible.

Here we report results from three overarching objectives of this study: 1) to develop a novel mouse model of RT-induced cardiotoxicity involving PH irradiation 2) to characterize the pathophysiologic mechanisms of cardiotoxicity in the model, and 3) to use the model to identify biomarkers of cardiac injury.

MATERIALS AND METHODS

Mice

Female 9–11-week-old C57BL/6 mice (The Jackson Laboratory) were maintained in our institution’s animal facilities. All experimental procedures were conducted in accordance with the guidelines and protocols approved by the Institutional Animal Care and Use Committee. Mice were subjected to image-guided RT using the Small-Animal Radiation Research Platform (SARRP, Xstrahl Life Sciences) and irradiated with a single dose of 20, 40 or 60 Gy. Mice were euthanized at various time points specified below to collect plasma and heart and lung tissues for further analysis. Three or more mice were used in each group for any given study.

Cone-beam computed tomography (CBCT) imaging and RT

For these studies, all mice received a single 200 uL tail vein injection of a blood pool contrast agent (FenestraVC, MediLumine Inc., Montreal, Canada) to visualize the heart on cone-beam CT (CBCT) imaging prior to irradiation. Each mouse was imaged and irradiated while immobilized with 2.5% isoflurane anesthesia with medical air as the carrier gas (VetEquip). Following 5 minutes in an induction chamber, the fully anesthetized mouse was placed on a customized platform in the ventral recumbent position. The head of the mouse was placed in a face mask that allows the gas to be scavenged (Xerotec Inc.). The platform was placed off the stage of the SARRP. Using the SARRP Control Interface, a CBCT image was initiated with the X-ray tube operating at 65 kV, 0.5 mA with aluminum filtration approximately 5–15 minutes post-FenestraVC administration. The images were reconstructed with Xstrahl's MuriSlice Software. Dosimetry was performed by measuring EBT2 gafchromic film exposure, at depth using solid-water phantom material, with a Microtek Artixcam M1 camera. The dose-exposure calibration was done using a cesium irradiator with calibration dose rate.

To carry out PH irradiation, an isocenter was selected on the contrast-enhanced CBCT at the posterolateral cardiac wall (left ventricular (LV) wall) approximately 2–3 mm superior to the cardiac tip for targeted RT using the software. Once the isocenter was determined, the robotic stage moved the animal to the proper location. Single doses of 20, 40, or 60 Gy of photon RT were precisely delivered to the cardiac apex with or without including adjacent lung tissue, using a 3×3mm collimated beam operating at 220 kV, 13 mA with copper filtration. Each dose was calculated and prescribed using tissue segmentation and heterogeneity corrections for soft tissue and air densities. The dose rate was 1.65 Gy/minute.

γ-H2AX and Masson's trichrome staining

Details of sample processing and staining are given in Supplementary Materials. Quantification of cardiac fibrosis on trichrome staining at 8 weeks and 24 weeks post-RT was performed using the Aperio ImageScope 12.4.3 – Pathology Slide Viewing Software. Five sections separated by 100 uM were used for fibrosis quantification of each mouse heart. For each section, whole heart fibrosis was calculated by drawing an area of interest around the entire stained cardiac tissue. Additionally, the thickness of cardiac vessels in the apical half of the heart (irradiated region) were calculated by measuring the distance from the lumen of the vessel to the edge of the perivascular fibrotic or connective tissue. Depending on vessel size and uniformity, 4–20 measurements were taken per vessel and then averaged.

Biochemical marker and cytokine quantification

Mouse cardiac tissue homogenates were analyzed for troponin T, troponin I, PlGF, interleukin (IL)-2, IL-6, and tumor necrosis factor-alpha (TNFα) levels. Human and mouse plasma samples were also analyzed for these marker levels. Details are given in Supplementary Materials.

Mouse plasma collection

Whole blood was collected into heparinized collecting tubes (Fisher Scientific, 02–668-10) also containing EDTA, from cardiac puncture in terminal experiments or the tail vein of the

mice in non-terminal experiments at 1, 2, 4, and 8 weeks post-RT. Plasma was obtained by centrifugation for 10 minutes at 1,500 rpm using a refrigerated centrifuge. Plasma samples were aliquoted and stored at −80 °C.

Human plasma collection and sample selection

A random selection of human plasma samples from patients who were treated with thoracic RT and who were enrolled in a prospective longitudinal cohort study (IRB#808014) conducted at our institution from June 2015 until February 2018 were obtained. Details of the study population and methods have been previously reported.[16] Briefly, blood samples were collected pre- and post-RT (median, 20 days) and stored at −80 °C. A total of 14 patients with lung cancer and 32 patients with breast cancer had plasma samples available both pre- and post-RT and were used in this study. Only 4 patients with mediastinal lymphoma had pre- and post-RT plasma samples available, with most samples yielding undetectable biomarker levels on analysis. These samples were therefore excluded from the study.

Quantitative echocardiography

Ultrasound examination of the left ventricle (LV) was performed at 4, 8, and/or 16 weeks post-RT using a Fujifilm VisualSonics Ultrasound System (VisualSonics Inc, Toronto, ON, Canada) and using an MS400 (18–38 MHZ) transducer. Mice were lightly anesthetized with an intraperitoneal injection of 0.005 ml/g of 2% Avertin (2,2,2-Tribromoethanol, Sigma-Aldrich, St. Louis, MO). Hair was removed from the anterior chest using chemical hair remover (Nair), and the animals were placed on a warming pad in a left lateral decubitus position to maintain normothermia (37°C), monitored by a rectal thermometer. Ultrasound gel was applied to the chest. Care was taken to maintain adequate contact while avoiding excessive pressure on the chest. Two-dimensional long-axis, short-axis M-Mode images were obtained to evaluate LV systolic function. Trans mitral inflow pattern and tissue Doppler were obtained in modified 4 chamber apical view to evaluate LV diastolic function. After completion of the imaging studies, mice were allowed to recover from anesthesia and returned to their cages. M Mode Images were analyzed for LV structure and function related parameters and Pulse wave and tissue Doppler images were analyzed for diastolic function related parameters using Vevo Lab software (Visual Sonics Inc, Toronto, ON, Canada). Analyses were performed blinded to treatment group.

Tc-99m sestamibi SPECT

SPECT imaging was performed at 8 weeks post-RT under continuous isoflurane gas anesthesia by the nose cone. While under anesthesia, mice were injected via tail vein with 4–7mL Cu (volume <10% body weight of animal) of a radioactive tracer, Tc-99m sestamibi (Nuclear Diagnostic Products), and scanned on the small animal SPECT system (MILabs USPECT) approximately 5–10 minutes after injection. Mice were placed in the approved radioactive decay room until they were no longer radioactive (10 half-lives of the isotope).

Images were reconstructed with a reconstruction program (U-SPECT-Rec2.51g) provided by MiLabs. The reconstruction parameters were: 0.4 mm voxel size, 4 subsets, 6 iterations, 0.25 FWHM Gaussian post filter for all images.

LV wall perfusion was qualitatively and quantitatively assessed using MIM Software Inc. Quantitative assessment was carried out by subdividing LV walls into apical and basal components for the anterior, inferior, lateral, and septal walls. The software was used to contour the specific LV wall segments and quantify regional tracer uptake. Individual LV wall tracer concentration values obtained were normalized to activity of tracer injected or blood pool tracer concentration in separate analyses.

Statistical analysis

Statistical analyses were performed with GraphPad Prism version 8 (GraphPad Software, La Jolla, CA) and Microsoft Excel. Data are presented as means ± standard error of the mean (SEM). Results were considered statistically significant when $p<0.05$ by the appropriate test (unpaired Student's t-test). A one-sample t-test was used to assess for significant fold changes in marker levels pre- and post-RT. Linear regression was used to evaluate for significant correlations between fold change in marker levels pre -and post-RT and mean heart RT dose. Fisher's exact test was utilized for comparison of fold changes in marker levels pre- and post-RT in lung cancer versus breast cancer patients. The threshold was set at >30% change over pre-RT levels.[16]

RESULTS

Mouse model for RT-induced localized heart damage

The first objective of this study was to develop a reproducible mouse model of targeted PH irradiation. The treatment schemes implemented are depicted in Figure 1. RT planning was done on contrast enhanced CBCT images 5–10 minutes post-FenestraVC tail vein injection (Supplementary Fig. S1). PH irradiation was first performed at 20 Gy, (n=12) a typical dose for small animal thoracic RT studies, using a single 3×3mm beam angled at 15° to the horizontal (Supplementary Fig. S2A). To evaluate direct DNA damage post-RT and RT targeting, sections of heart and lung tissue were stained for γ-H2AX (n=4). The phosphorylation of histone H2AX at serine 139 (γ-H2AX) is a well-known, early effect of RT exposure, and the presence of γ-H2AX is considered a sensitive and quantitative marker of DNA double-strand breaks. Results from the immunofluorescence staining of heart tissue for γ-H2AX at one hour post-RT confirmed DNA damage is restricted to the 3×3mm area in the lower third of the heart (cardiac apex) (Supplementary Fig. S2B), leaving the surrounding tissues intact. As the RT target volume was significantly smaller than that in previously reported studies, we hypothesized that higher doses would not only be well-tolerated, but might also be necessary to elicit significant, detectable cardiac injury within a practical timeframe. Indeed, no qualitative abnormalities on the histopathologic analysis described below were identified post-20 Gy PH RT at 8 and 24 weeks of follow-up (n=4 each). Therefore, subsequent studies were conducted at doses ≥ 40 Gy.

To deliver doses of 40 Gy (n=20) and 60 Gy (n=20) while minimizing skin toxicity and ulceration, we used a novel RT plan based on our treatment scheme for 20 Gy PH RT, involving conformal RT delivered over a 75° arc, again using a 3×3mm beam (Fig. 2A and B). This treatment scheme reduced the maximum dose delivered to the skin almost two-fold (Supplementary Fig. S2B). Lastly, to evaluate the potential indirect effects of lung

irradiation on cardiac injury, PHL irradiation to 40 Gy (n=20) involving approximately 40% of the left lung volume was carried out using two opposing anterior-posterior posterior-anterior (AP/PA) 3×3mm beams, each delivering a 20 Gy dose to the isocenter selected at the LV apical wall (Fig. 2C and D). The increase in RT dose delivery to the lung with this treatment scheme can be seen in Supplementary Fig S2B. Corresponding staining at one hour post-conformal RT to 40 and 60 Gy revealed localized DNA damage extending up to 1 mm beyond the 3×3mm border in the lower third of the heart (Supplementary Fig. S2B), in the area of dose fall off. Results from lung tissue staining post-conformal RT confirmed the absence of lung tissue DNA damage (Fig. 2D and E). Conversely, clear and localized DNA damage confined to a 3×3mm area in the left lung was detected in the RT scheme involving AP/PA beams (Fig. 2F).

Mean heart dose for 40 Gy PH-, 40 Gy PHL-, and 60 Gy PH- treated mice were 5.7 Gy, 4.8 Gy, and 8.7 Gy, respectively. Corresponding values for mean partial heart dose (dose RT beam targeting) were 39 Gy, 38 Gy, and 59 Gy. No deaths were observed in any of the treatment schemes and all the mice continued gaining weight post-RT (Supplementary Fig. S3).

Development of cardiac fibrosis and vascular damage

RT-induced damage can develop chronically, and in most normal tissues is characterized by collagen deposition and excessive formation of fibrous tissue, at which point damage is considered irreversible. Therefore, we evaluated the levels of fibrosis in cardiac tissue at 8 and 24 weeks post-RT using Masson's trichrome staining. Figure 3A shows representative trichrome staining at 8 weeks post-RT, and Figure 3B shows results from fibrosis quantification at 8 and 24 weeks post-RT. Although increased at 8 weeks post-RT, fibrosis levels only reached statistical significance at 24 weeks post-RT: 0 Gy (% fibrosis = 1.0) 40 Gy PH (1.4%, p=0.079), 40 Gy PHL (2.0%, p=0.022) and 60 Gy PH (1.5%, p=0.017). Surprisingly, and in contrast to studies reporting the development of diffuse myocardial fibrosis in irradiated areas of tissue, we found that fibrosis was primarily located in perivascular regions (Fig. 3C), with only mild interstitial fibrosis concentrated in the lower half of the heart (roughly the area of irradiation). To further characterize differences in the cardiac vasculature between irradiated and non-irradiated mice, we quantified cardiac vessel wall thickness in the area of irradiation at 8 and 24 weeks post-RT. Compared to control (11.4 μm ± 1.4), average vessel wall thickness was most increased at 24 weeks post 40 Gy PH (13.4 μm ± 1.2, p=0.347), 40 Gy PHL (18.4 μm ± 0.7, p=0.005) and 60 Gy PH RT (28.9 μm ± 1.7, p<0.001) (Fig. 3D).

Dose- and time-dependent mechanistic cardiac dysfunction

Current recommendations for managing potential cardiac dysfunction in patients receiving cardiotoxic therapies heavily rely on LVEF monitoring with serial echocardiograms. As such, we implemented echocardiography at 4 weeks post-60 Gy RT (Supplementary Fig. S4), and also at 8 and 16 weeks in all cohorts (Fig. 4A and B) to evaluate functional changes in the heart. Qualitatively, RT resulted in dose-dependent, progressive cardiac dysfunction, as indicated by hypokinesis at the cardiac apex. (Supplementary Video S1). There were no significant differences in heart rate across groups.

LVEF and E/e' (ratio of mitral peak velocity of early filling (E) to early diastolic mitral annular velocity (e′)) were used as measures of systolic and diastolic dysfunction, respectively (Supplementary Table S1). Compared to non-irradiated mice (LVEF = 68.0% ± 1.2, 67.3% ± 1.2 and 69.7% ± 3.2 at 4, 8, and 16 weeks post-RT, respectively), LVEF was decreased at 8 (62.2% ± 0.6, p=0.012) and 16 (62.8% ± 4.0, p=0.006) weeks post-40 Gy PH RT, at 8 (63.8% ± 1.5, 0.090) and 16 (63.8% ± 4.0, p=0.011) weeks post-40 Gy PHL RT, and at 4 (61.9%± ± 2.0, p=0.068), 8 (53.5% ± 2.3, p<0.001) and 16 (55.2% ± 3.6, p<0.001) weeks post-60 Gy PH RT. Compared to control (E/e' = 28.2 ± 2.2 and 27.5 ± 4.5 at 8 and 16 weeks post-RT, respectively), E/e' was significantly increased, indicative of diastolic dysfunction, at 16 weeks post-40 Gy PHL RT (38.8 ± 4.9, p=0.002) and at 8 (36.4 ± 0.9, p=0.002) and 16 (40.1 ± 2.3, p<0.001) weeks post-60 Gy PH RT.

To evaluate for progressive, time-dependent LVEF and E/e' changes post-RT, we analyzed changes within each treatment group. For LVEF, we only observed significant, progressive LVEF decreases in the 60 Gy PH RT cohort from 4 to 8 weeks post-RT (p=0.016). E/e', however, significantly increased from 8 to 16 weeks post-40 Gy PH RT (p=0.026) and 40 Gy PHL RT (p=0.011), and 4 to 8 (p=0.030) and 4 to 16 (p=0.022) weeks post-60 Gy RT. The remaining parameters measured with echocardiography are shown in Supplementary Fig S5.

Dose- and site-dependent decrease in myocardial perfusion

It is well established that SPECT imaging with Tc-99m sestamibi is a useful imaging modality to identify LV wall perfusion deficits.[19] Therefore, we carried out cardiac SPECT imaging at 8 weeks post-RT to provide insight into the physiologic basis for the observed echocardiographic abnormalities. Compared to control, dose-dependent LV apical perfusion deficits were observable post-RT (Fig. 5A). Upon segmentation and contouring of the LV basal and apical walls (Supplementary Fig. S6), quantification of tracer uptake normalized to tracer activity injected revealed a modest fold change reduction in myocardial perfusion in the LV base, with greater fold change reduction in the LV apex post 40 Gy PH (0.839 ± 0.1, p=0.342), 40 Gy PHL (0.602 ± 0.04, p=0.006), and 60 Gy PH (0.494 ± 0.03, p=0.002) RT compared to control (1.0 ± 0.1) (Fig. 5B, Supplementary Table S2A). Similar results were observed when LV wall tracer uptake was normalized to blood pool tracer concentration (Supplementary Table S2B).

Cardiomyocyte and vascular stress and systemic inflammatory response

Analysis of biomarkers of heart damage in situ and in circulating blood was another objective of this study. Thus, we evaluated irradiated segments of cardiac tissue from mice and plasma from both humans and mice for known and novel markers of cardiac damage, vascular injury, and inflammation at various timepoints post-RT (Fig. 6, Supplementary Table S3, Supplementary Fig. S7). In irradiated cardiac tissue, troponin T and PlGF significantly decreased and increased, respectively, at various timepoints between 1 and 8 weeks post-40 Gy PHL and post-60 Gy PH RT, with PlGF also significantly increased post 40 Gy PH RT. The inflammatory markers evaluated, IL-2, IL-6, and TNFα, showed the most significant increases in cardiac tissue compared to control following concomitant PHL RT (Fig. 6A). These findings prompted a corresponding analysis to be conducted in the plasma of patients who received breast (mean heart dose 1.5 Gy) and lung (mean heart dose

8.6 Gy) RT, which showed significant increases in PlGF (p=0.021) and TNFα (p=0.036) post- lung RT (Fig 6B). Additionally, the fold change in PlGF was found to be significantly correlated with mean heart dose in the lung cancer subgroup (r=0.89, p=0.0001) (Fig. 6B). Corresponding analysis in the breast cancer subgroup did not reveal significant correlations (data not shown here), and when compared to the lung cancer subgroup, showed significantly decreased occurrence of PlGF (p=0.0118) and TNFα (0.0008) increases post-RT (Fig 6C). Data from plasma analysis in mice and additional plasma biomarker analysis in humans is shown in Supplementary Fig. S7.

DISCUSSION

In the current study, we have developed and implemented a novel mouse model of image-guided RT-induced cardiac damage to study the molecular and cellular pathophysiology of RIHD, and to identify sensitive biomarkers of disease development. Using a contrast agent to improve visualization of cardiac substructures on CBCT imaging prior to RT, we were able to carry out PH irradiation similar to that encountered in clinical practice. Additionally, we were able to use the model to demonstrate dose- and site-dependent RT-induced damage on radiologic, biochemical, and histologic analyses.

To our knowledge, this is the first mouse model of PH irradiation which implements cardiac conformal RT, building upon other existing models and offering several unique advantages. First, the model only requires a single tail vein injection of the FenestraVC contrast agent, which aids in RT beam targeting through improving visualization of cardiac borders. While necessary for most current SARRP instruments, contrast agent injection may prove to be unnecessary in future studies as preliminary implementation of a more advanced SARRP instrument has already shown adequate unenhanced CT resolution, thus increasing the potential feasibility and cost-effectiveness of this model. Second, the use of cardiac conformal RT in a mouse is itself a novel technological innovation, since it enables high dose delivery without significant skin toxicity. The PH RT design not only mimics the cardiac RT exposure of thoracic radiation oncology patients, but it may also enable the investigation of targeted radioablation for refractory cardiac arrhythmias, a non-oncologic use of RT that is rapidly being incorporated into clinical practice. Lastly, although not tested in this study, our model is also amenable to fractionated delivery of RT, which may further increase its clinical relevance.

Prior mouse models of RIHD have been valuable in determining dose-dependent effects of cardiac dysfunction and have provided insights into the pathophysiological parameters involved in disease progression.[20] However, they have been limited by the fact that they involved either whole thorax or whole heart and partial lung RT. In addition to such treatment plans not being used clinically, there is also an increased risk of death of the irradiated mice at early timepoints, before long-term toxicities such as fibrosis, which can take months to develop depending on the dose and irradiated area, have manifested. Lee et al. carried out PH irradiation in Tie2Cre; p53(FL/-) and Tie2Cre; p53(FL/+) mice, however, due to significant dose constraints (12 Gy), no cardiac damage was detectable on imaging or histology of wild type mice over 8 weeks of follow-up.[21] It should be noted that in our experiments, no mice died due to RT toxicity over 24 weeks of follow-up despite the

very high RT doses eliciting detectable cardiac damage. This finding underscores a volume and dose effect on mortality post-thoracic RT. It also affords the opportunity to study long-term effects of RT-induced damage, which is especially useful in studies of cardiovascular damage, which often develops more chronically than damage in other organs.

An important feature of preclinical models of RT-induced cardiotoxicity is the ability to histologically evaluate cardiac tissue,[8, 22] an analysis which can rarely be done in humans. A novel, previously unreported histologic finding from our study is the appearance of significant fibrosis primarily in perivascular regions and largely absent from other areas. Trichrome staining revealed clear vessel wall thickening and morphologic changes, with only scattered areas of interstitial fibrosis and no evidence of replacement fibrosis, suggesting a potential degree of cardiomyocyte radioresistance relative to cardiac vascular endothelium. If validated in human patients, this finding may be useful in guiding prioritization selection of dosimetric constraints in thoracic RT planning – i.e. mean heart dose versus mean left anterior descending arterial dose.[23] Additionally, we were able to elucidate the topography of the RT-induced damage, which at higher doses and with radiation exposure of lung tissue extended beyond the small area of RT, consistent with both direct and systemic components to the RT-induced damage. Indeed, while localized cardiac damage, as evidenced by increased vessel wall thickness in the irradiated portion of the heart, was greatest post 60 Gy PH, total cardiac fibrosis was actually greatest post lower dose PHL RT. Lastly, it is worth noting that significantly higher doses of RT were necessary to elicit histologic abnormalities when compared to previous studies of whole heart or whole thorax RT, which report histopathologic changes at doses ranging from 16–24 Gy.[10, 11, 24] Given the smaller volume of irradiated tissue, and the relative sparing of large vessels and valves (ascending aorta and valve) reported in this model, this provides evidence in support of both volume of RT and vessel/valve radiation exposure as significant driving factors in the development of cardiac injury, and further characterization of the dose response curve and maximum tolerated/lowest significant dose could be useful. As the current study exclusively involves RT of the cardiac apex (chosen primarily to minimize dose to critical cardiac vessels and structures during initial development of the model, and to achieve maximal lung RT sparing in the PH treatment scheme) future studies involving RT of the cardiac base and ascending aorta would be valuable in elucidating potential differences in resulting cardiotoxicity.

At present, there is great interest in implementing radiologic studies to analyze both acute and chronic effects of radiation-induced cardiotoxicity and identify sensitive biomarkers of disease development. Through the use of quantitative echocardiography, we were able to identify systolic and diastolic dysfunction. However, studies have reported mixed results in both humans[12, 16] and animal models[10, 25] with echocardiography post-RT, whose value is often limited to characterizing cardiac function.[12, 16] SPECT imaging represents an attractive diagnostic approach, as it has demonstrated significant utility in assessing myocardial perfusion.[19, 26] The gross perfusion deficits in the area of RT, and the global decrease in perfusion observed in our study provide evidence for a significant vascular component to RT-induced cardiac injury, and was corroborated histologically by vessel wall thickening and fibrosis. Further evaluation of SPECT for the diagnosis of cardiac perfusion

abnormalities and risk stratification of thoracic RT patients would be a useful undertaking for the detection of subclinical cardiotoxicity.

In this study, we also analyzed levels of several markers of myocardial injury, vascular damage, and inflammation. While troponin has routinely been used to diagnose cardiac injury of varying etiologies, studies have failed to demonstrate consistent and significant associations between increased troponin levels and RT-induced cardiac damage.[23, 27, 28] One explanation for this is that, as our study demonstrates, cardiac injury may be primarily mediated by vascular endothelial cell injury and associated inflammation, as opposed to direct myocardial damage. PlGF, a vascular endothelial growth factor (VEGF) homologue, has been shown to play crucial roles in atherogenic lesion formation and cardiac vessel wall thickening, and studies have reported its potential role in the progression of cardiovascular disease in the general population.[29, 30] More recently, blood PlGF levels have also been evaluated prospectively in thoracic RT patients, and post-RT PlGF was found to be increased in lymphoma and lung cancer patients, and associated with mean heart radiation dose, V5, and V30 (percent volume of heart receiving 5 Gy and 30 Gy, respectively). Additionally, acute increases in inflammatory cytokines post-RT is well-characterized in multiple tissues.[18, 31, 32] As such, we conducted a multiparametric analysis of PlGF, IL-2, IL-6, IL-10, and TNFα, which showed significant increases in the cardiac tissue and/or plasma of irradiated mice compared to that of non-irradiated mice. These findings were corroborated in preliminary human plasma studies, with PlGF and TNFα showing significant increases post-lung RT and PlGF fold changes significantly correlating with mean heart dose, These results not only support the clinical relevance of our model but also highlight the potential for use of these markers to identify cardiac injury in clinical care. Furthermore, as we observed greater marker level changes (particularly PlGF level changes) in lung cancer patients (higher mean heart doses) compared to breast cancer patients, future studies could investigate the specificity of PlGF increases for cardiac RT by evaluating plasma samples pre- and post- non-cardiac RT (liver, intestine, prostate, etc.).

A particularly noteworthy observation was the greater increase in inflammatory markers following PHL irradiation (40 Gy RT) compared to higher-dose PH irradiation alone (60 Gy conformal RT). This suggests that lung irradiation may indirectly cause cardiac damage by stimulating a more robust inflammatory response. To date, numerous studies in humans have demonstrated a significant relationship between pulmonary toxicity (e.g. radiation pneumonitis) and the release of inflammatory cytokines following lung RT.[33–35] However, similar data on the potential indirect effects of lung RT on the heart are lacking. Future investigation in cytokine (e.g. IL-6) knockout mice may be useful in elucidating a causative role of inflammatory mediators. Additionally, future histopathologic analysis of lung tissue post- PH and PHL RT could more robustly correlate cardiac dysfunction and the degree of pulmonary injury. Nevertheless, when taken together with our radiologic and histologic findings, our results provide evidence for a strong vascular component to radiation-mediated cardiotoxicity, and a potential role of lung irradiation in eliciting an inflammatory cascade causing cardiac damage.

Our study has a number of limitations, one being the fact that RT was delivered to a beating heart and breathing mouse, creating some degree of variability in RT targeting and delivery.

Additionally, in order to elicit detectable cardiac damage within a practical timeframe, we delivered RT at doses of 40–60 Gy, which are significantly greater than heart RT doses patients typically receive; nevertheless, now that we have established and characterized a novel model, lower dose RT experiments with longer periods of follow up (1–2 years) could potentially offer more clinically relevant insights. Another limitation is the use of single fractionation RT. However, future studies could implement multiple fractionation RT, or even newer RT modalities to characterize differences in pathophysiology. Furthermore, the model is amenable to the study of radiosensitizers and radioprotectors, (such as anti-fibrotic agents, including anti-TGF-beta antibody and anti-inflammatory agents including anti-IL-6 antibody), which could eventually be used to directly influence clinical care. Lastly, given the limited number of patients included in the human plasma biomarker analysis, further validation in larger cohorts is needed prior to implementation in the clinic.

In conclusion, we have developed a novel mouse model of PH irradiation with or without lung irradiation as a new preclinical tool to study clinically relevant RT-induced cardiotoxicity. In addition, we used our model to gain insight into relevant pathophysiologic mechanisms, and identified significant changes in myocardial function and perfusion and vascular and inflammatory biomarkers post-RT. Thus, the model can be used for identification of clinically targetable biologic mediators and ultimately contribute to better strategies for surveillance and treatment of disease.

Supplementary Material

Refer to Web version on PubMed Central for supplementary material.

ACKNOWLEDGEMENTS

The authors acknowledge the Small Animal Imaging Facility and the Veterinary School of Medicine at the University of Pennsylvania for their invaluable contributions to this study. The authors also thank the University of Pennsylvania Diabetes Research Center for the use of the Biomarkers Core (P30-DK19525). A.D.D. was supported by a fellowship from the National Center for Advancing Translational Sciences of the National Institutes of Health (TL1TR001880). B.K was supported by R01 HL 118018 (Ky) and B.K and S.J.F by R01 HL148272 (Ky). This work was partially supported by a grant to C.K. from the Cardio-Oncology Translational Center of Excellence of the Abramson Comprehensive Cancer Center and by developmental funds from the Department of Radiation Oncology at the University of Pennsylvania.

Financial support:

National Center for Advancing Translational Sciences of the National Institutes of Health (TL1TR001880) and R01 HL148272, and Penn Cardio-Oncology Translational Center of Excellence and Thalheimer Center for Cardio-Oncology pilot grant

REFERENCES

1. Delaney G, Jacob S, Featherstone C, Barton M. The role of radiotherapy in cancer treatment: estimating optimal utilization from a review of evidence-based clinical guidelines. Cancer 2005;104: 1129–1137. [PubMed: 16080176]
2. Ghobadi G, van der Veen S, Bartelds B, et al. Physiological interaction of heart and lung in thoracic irradiation. Int J Radiat Oncol Biol Phys 2012;84: e639–646. [PubMed: 22975617]
3. Darby SC, Ewertz M, Hall P. Ischemic heart disease after breast cancer radiotherapy. N Engl J Med 2013;368: 2527.

4. Eaton BR, Pugh SL, Bradley JD, et al. Institutional Enrollment and Survival Among NSCLC Patients Receiving Chemoradiation: NRG Oncology Radiation Therapy Oncology Group (RTOG) 0617. J Natl Cancer Inst 2016;108.
5. Han X, Zhou Y, Liu W. Precision cardio-oncology: understanding the cardiotoxicity of cancer therapy. NPJ Precis Oncol 2017;1: 31. [PubMed: 29872712]
6. Spetz J, Moslehi J, Sarosiek K. Radiation-Induced Cardiovascular Toxicity: Mechanisms, Prevention, and Treatment. Curr Treat Options Cardiovasc Med 2018;20: 31. [PubMed: 29556748]
7. Boerma M Experimental radiation-induced heart disease: past, present, and future. Radiat Res 2012;178: 1–6. [PubMed: 22663150]
8. Boerma M, Wang J, Wondergem J, et al. Influence of mast cells on structural and functional manifestations of radiation-induced heart disease. Cancer Res 2005;65: 3100–3107. [PubMed: 15833839]
9. Boerma M, Roberto KA, Hauer-Jensen M. Prevention and treatment of functional and structural radiation injury in the rat heart by pentoxifylline and alpha-tocopherol. Int J Radiat Oncol Biol Phys 2008;72: 170–177. [PubMed: 18632215]
10. Mezzaroma E, Di X, Graves P, et al. A mouse model of radiation-induced cardiomyopathy. Int J Cardiol 2012;156: 231–233. [PubMed: 22340985]
11. Sievert W, Stangl S, Steiger K, Multhoff G. Improved Overall Survival of Mice by Reducing Lung Side Effects After High-Precision Heart Irradiation Using a Small Animal Radiation Research Platform. Int J Radiat Oncol Biol Phys 2018;101: 671–679. [PubMed: 29680258]
12. Stoodley PW, Richards DA, Hui R, et al. Two-dimensional myocardial strain imaging detects changes in left ventricular systolic function immediately after anthracycline chemotherapy. Eur J Echocardiogr 2011;12: 945–952. [PubMed: 21965152]
13. Maity A, Kao GD, Muschel RJ, McKenna WG. Potential molecular targets for manipulating the radiation response. Int J Radiat Oncol Biol Phys 1997;37: 639–653. [PubMed: 9112463]
14. Darby SC, Cutter DJ, Boerma M, et al. Radiation-related heart disease: current knowledge and future prospects. Int J Radiat Oncol Biol Phys 2010;76: 656–665. [PubMed: 20159360]
15. Ky B, Putt M, Sawaya H, et al. Early increases in multiple biomarkers predict subsequent cardiotoxicity in patients with breast cancer treated with doxorubicin, taxanes, and trastuzumab. J Am Coll Cardiol 2014;63: 809–816. [PubMed: 24291281]
16. Demissei BG, Freedman G, Feigenberg SJ, et al. Early Changes in Cardiovascular Biomarkers with Contemporary Thoracic Radiation Therapy for Breast Cancer, Lung Cancer, and Lymphoma. Int J Radiat Oncol Biol Phys 2019;103: 851–860. [PubMed: 30445173]
17. Gomez DR, Yusuf SW, Munsell MF, et al. Prospective exploratory analysis of cardiac biomarkers and electrocardiogram abnormalities in patients receiving thoracic radiation therapy with high-dose heart exposure. J Thorac Oncol 2014;9: 1554–1560. [PubMed: 25521400]
18. Bell BI, Koduri S, Salas Salinas C, et al. Interleukin 6 Signaling Blockade Exacerbates Acute and Late Injury From Focal Intestinal Irradiation. Int J Radiat Oncol Biol Phys 2019;103: 719–727. [PubMed: 30336264]
19. Wu MC, Gao DW, Sievers RE, Lee RJ, Hasegawa BH, Dae MW. Pinhole single-photon emission computed tomography for myocardial perfusion imaging of mice. J Am Coll Cardiol 2003;42: 576–582. [PubMed: 12906991]
20. Boerma M, Hauer-Jensen M. Preclinical research into basic mechanisms of radiation-induced heart disease. Cardiol Res Pract 2010;2011.
21. Lee CL, Min H, Befera N, et al. Assessing cardiac injury in mice with dual energy-microCT, 4D-microCT, and microSPECT imaging after partial heart irradiation. Int J Radiat Oncol Biol Phys 2014;88: 686–693. [PubMed: 24521682]
22. Sridharan V, Thomas CJ, Cao M, et al. Effects of local irradiation combined with sunitinib on early remodeling, mitochondria, and oxidative stress in the rat heart. Radiother Oncol 2016;119: 259–264. [PubMed: 27072940]
23. Kuo AH, Ancukiewicz M, Kozak KR, Yock TI, Padera TP. Cardiac and inflammatory biomarkers do not correlate with volume of heart or lung receiving radiation. Radiat Oncol 2015;10: 5. [PubMed: 25573181]

24. Seemann I, Gabriels K, Visser NL, et al. Irradiation induced modest changes in murine cardiac function despite progressive structural damage to the myocardium and microvasculature. Radiother Oncol 2012;103: 143–150. [PubMed: 22112779]
25. Saiki H, Moulay G, Guenzel AJ, et al. Experimental cardiac radiation exposure induces ventricular diastolic dysfunction with preserved ejection fraction. Am J Physiol Heart Circ Physiol 2017;313: H392–H407. [PubMed: 28550173]
26. Underwood SR, Anagnostopoulos C, Cerqueira M, et al. Myocardial perfusion scintigraphy: the evidence. Eur J Nucl Med Mol Imaging 2004;31: 261–291. [PubMed: 15129710]
27. Hughes-Davies L, Sacks D, Rescigno J, Howard S, Harris J. Serum cardiac troponin T levels during treatment of early-stage breast cancer. J Clin Oncol 1995;13: 2582–2584. [PubMed: 7595710]
28. Serrano NA, Mikkelsen R, Canada J, Mezzaroma E, Weiss E, Abbate A. Biomarkers of cardiac injury in patients undergoing thoracic radiation therapy. Int J Cardiol 2016;223: 507–509. [PubMed: 27552565]
29. Khurana R, Moons L, Shafi S, et al. Placental growth factor promotes atherosclerotic intimal thickening and macrophage accumulation. Circulation 2005;111: 2828–2836. [PubMed: 15911697]
30. Lenderink T, Heeschen C, Fichtlscherer S, et al. Elevated placental growth factor levels are associated with adverse outcomes at four-year follow-up in patients with acute coronary syndromes. J Am Coll Cardiol 2006;47: 307–311. [PubMed: 16412852]
31. Lierova A, Jelicova M, Nemcova M, et al. Cytokines and radiation-induced pulmonary injuries. J Radiat Res 2018;59: 709–753. [PubMed: 30169853]
32. Verginadis II, R Kanade, B Bell, S Koduri, E Ben-Josef, C Koumenis. A Novel Mouse Model to Study Image-Guided, Radiation-Induced Intestinal Injury and Preclinical Screening of Radioprotectors. Cancer Res 2017;77: 908–917. [PubMed: 28011621]
33. Arpin D, Perol D, Blay JY, et al. Early variations of circulating interleukin-6 and interleukin-10 levels during thoracic radiotherapy are predictive for radiation pneumonitis. J Clin Oncol 2005;23: 8748–8756. [PubMed: 16314635]
34. Chen Y, Rubin P, Williams J, Hernady E, Smudzin T, Okunieff P. Circulating IL-6 as a predictor of radiation pneumonitis. Int J Radiat Oncol Biol Phys 2001;49: 641–648. [PubMed: 11172944]
35. Zhao L, Wang L, Ji W, et al. Elevation of plasma TGF-beta1 during radiation therapy predicts radiation-induced lung toxicity in patients with non-small-cell lung cancer: a combined analysis from Beijing and Michigan. Int J Radiat Oncol Biol Phys 2009;74: 1385–1390. [PubMed: 19231104]

Statement of Translational Relevance:

With the rising life expectancy of oncology patients, the long-term clinical consequences of radiation-mediated cardiotoxicity are becoming increasingly prevalent. Furthermore, the lack of effective diagnostic and therapeutic strategies has revealed a deficiency in the current data on the relevant pathophysiology. We developed a novel mouse model of partial heart irradiation, which revealed radiation-induced cardiac injury to be histologically characterized by perivascular fibrosis and vessel wall thickening. To define histopathologic and functional correlates, we implemented echocardiography and technetium-99 sestamibi SPECT and observed systolic and diastolic dysfunction and myocardial perfusion deficits post-radiation. Additionally, biochemical studies identified PlGF and TNFα as circulating markers of cardiac injury, and informed translational human studies in thoracic radiation patients, which corroborated these findings. Our model can uniquely facilitate the translation of preclinical findings into clinical practice, guiding targeted diagnostic and therapeutic interventions to decrease cardiovascular morbidity and mortality associated with treatment.

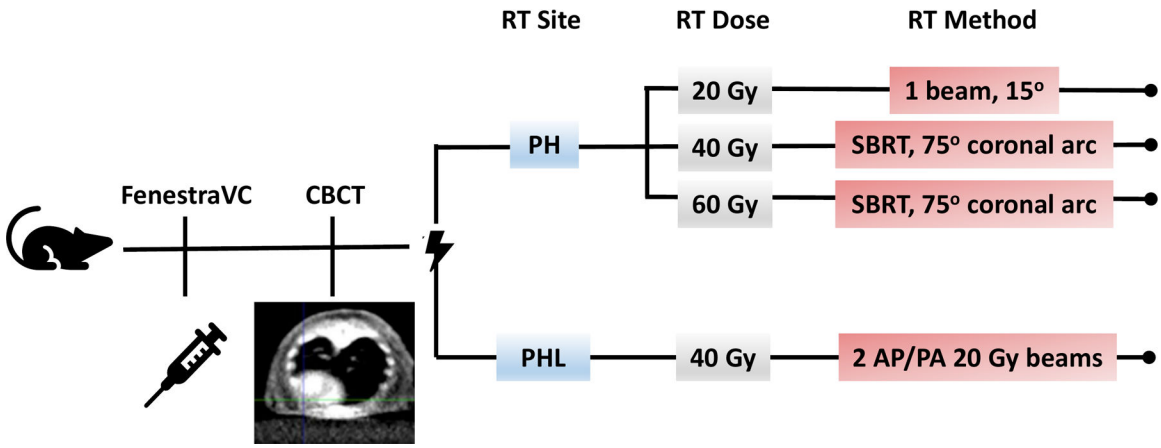

Figure 1. Schemes of cardiac irradiation.

All mice received the contrast agent FenestraVC through tail vein injection, followed by CBCT and radiation delivery. The radiation beam was targeted at the apex of the heart with a 3×3mm collimator at a dose of 20, 40, or 60 Gy, with conformal RT implemented at the latter two doses. Radiation was alternatively targeted at the apex of the heart and a portion of the left lung at a dose of 40 Gy using two opposing AP/PA 20 Gy beams.

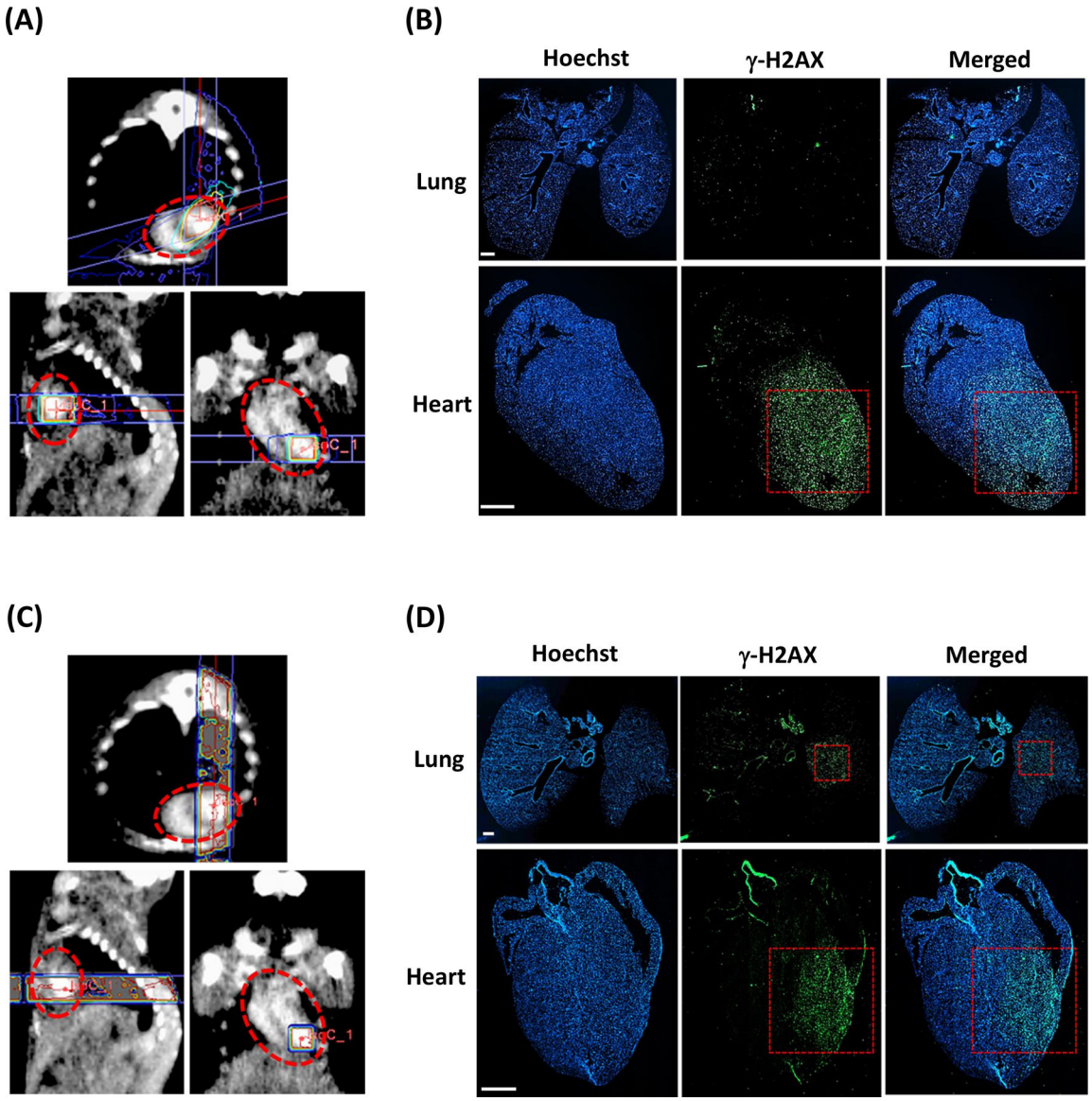

Figure 2. Dose plan in MuriPlan and corresponding immunohistochemical γ-H2AX staining of heart and lung tissue.

A, Axial, sagittal, and frontal views of RT planning and delivery to the cardiac apex at a dose of 60 Gy with a 3×3mm collimator and conformal RT over a 75° arc. **B,** Positive staining in the cardiac apex and negative staining in the lungs confirms selective PH RT targeting. **C,** Axial, sagittal, and frontal views of RT planning and delivery to the cardiac apex at a dose of 40 Gy using two 20 Gy 3×3mm vertical opposing beams. **D,** Positive staining in both the cardiac apex and in the mid-left lung confirms PHL RT targeting. The red dotted circles outline the cardiac silhouette. The red dotted boxes indicate the 3×3mm collimator. Scale bar 1mm.

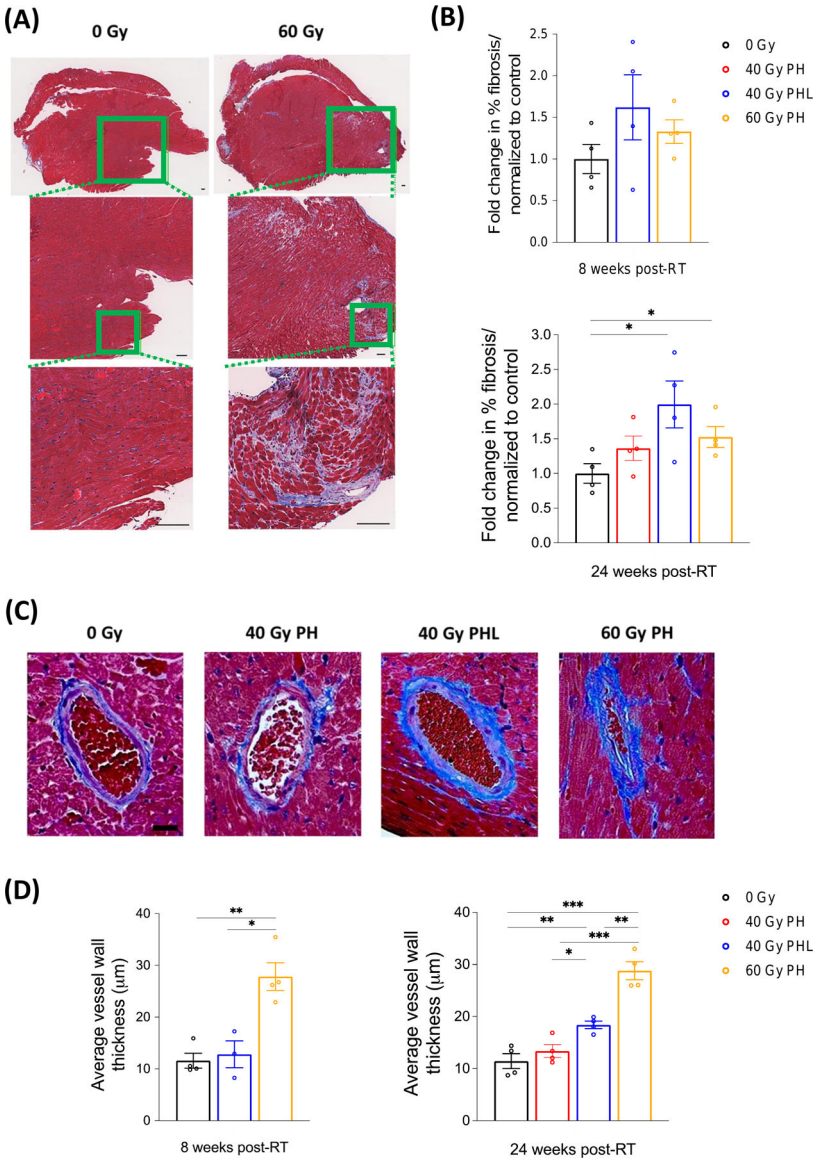

Figure 3. Masson's trichrome staining of cardiac tissue at 8 and 24 weeks post-RT.

A, Representative trichrome stains from 0 and 60 Gy cohorts at 8 weeks post-RT. Cardiac tissue is characterized by perivascular fibrosis superimposed on scattered interstitial fibrosis. Scale bar 100 µm. **B,** Quantification of fibrosis per measured area (n=4 per group). P=0.022 and 0.017 for 40 Gy PHL and 60 Gy PH cohorts, respectively. **C,** Representative vessels from each RT cohort showing perivascular fibrosis, vessel wall thickening, and lumen narrowing in irradiated cohorts 24 weeks post-RT. **D,** Quantification of vessel wall thickness in the lower half of the heart (irradiated region) (n=4 per group). At 8 weeks *P=0.022 and **P=0.002. At 24 weeks *P=0.013, **P=0.001 (60 Gy PH) and 0.005 (control), and ***P<0.001 (control and 40 Gy PH). Scale bar 20 µm.

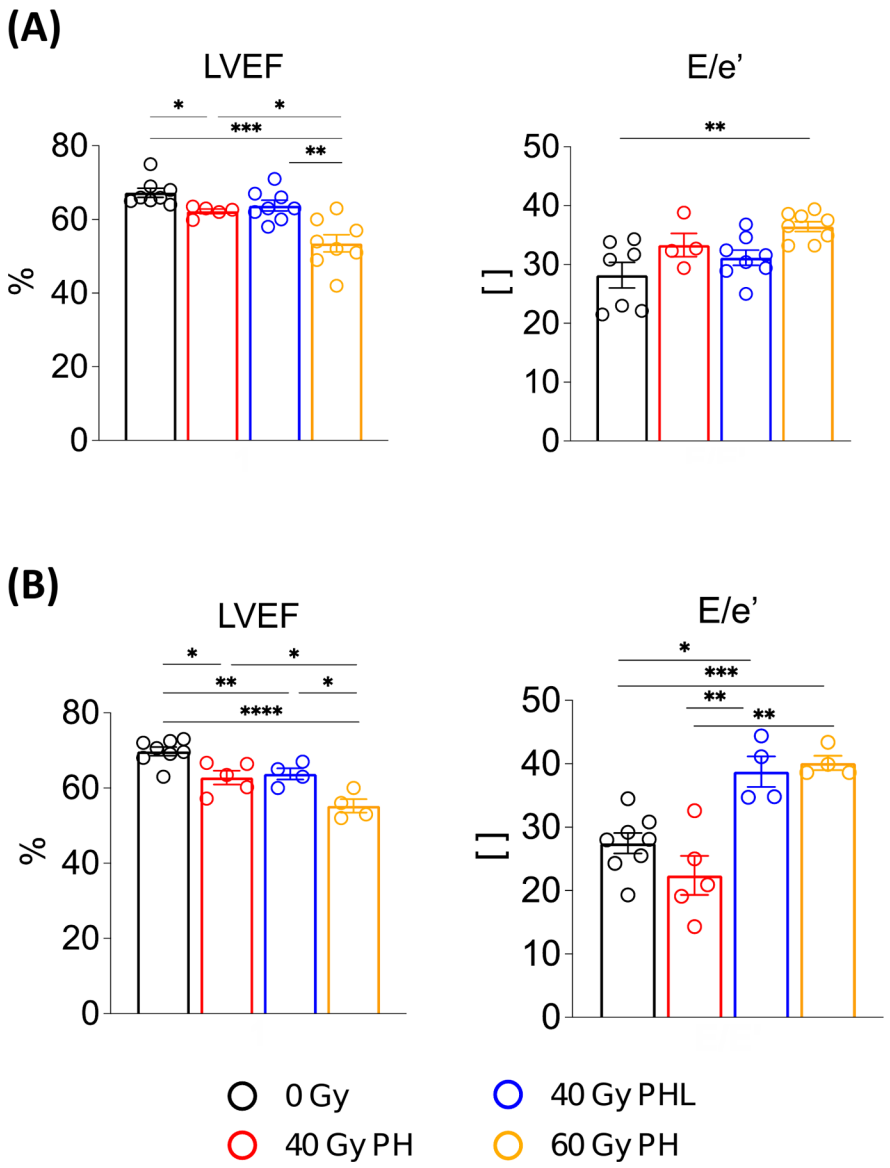

Figure 4. Quantitative echocardiography.

A, Comparison of cardiac systolic and diastolic functional parameters between irradiated and non-irradiated groups 8 weeks post-RT (*n* = 8, 5, 8, 8 per group). **B,** Corresponding comparison at 16 weeks post-RT (*n* = 8, 5, 4, 4 per group). *P<0.05, **P<0.01, ***P<0.001, ****P<0.0001 (details in supplementary Table S1). E/e′, ratio of mitral peak velocity of early filling (E) to early diastolic mitral annular velocity (e′).

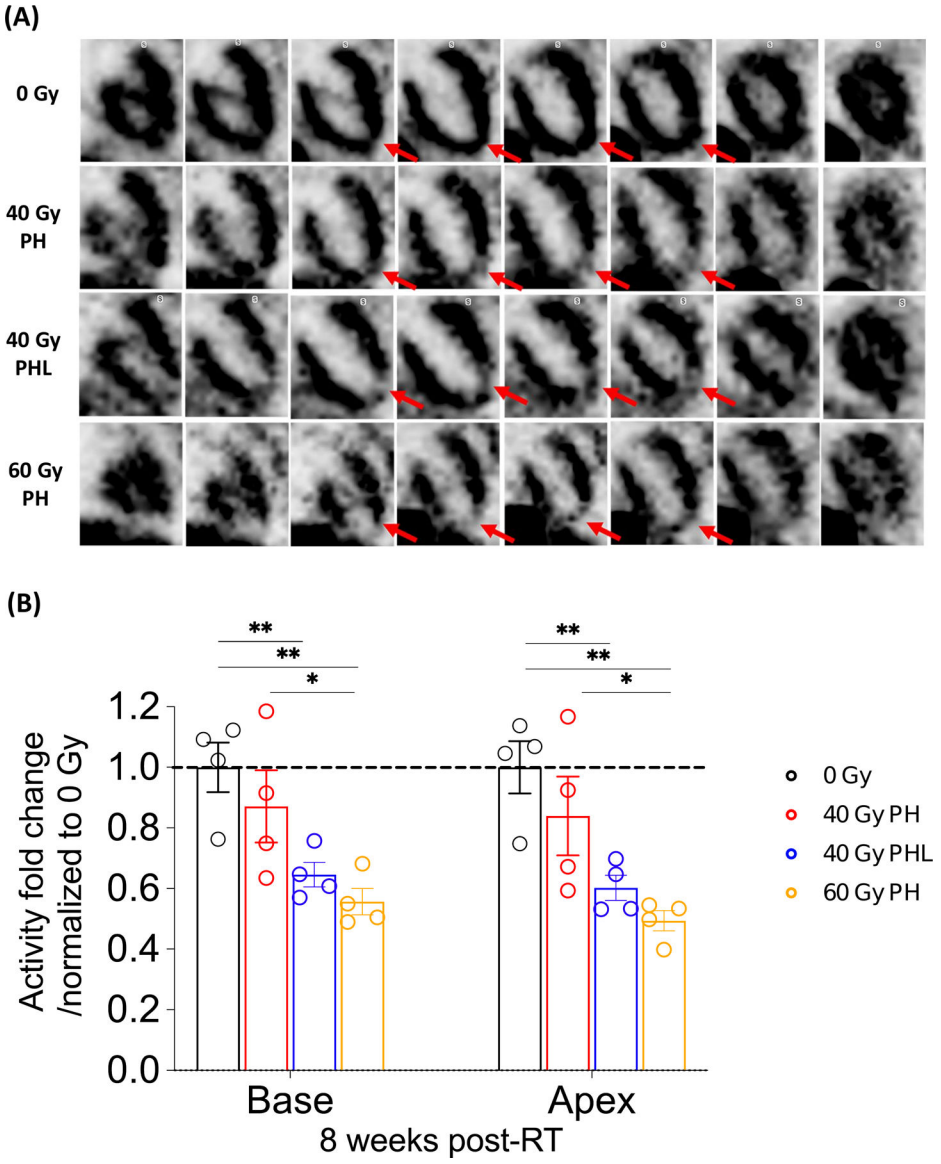

Figure 5. Tc-99 sestamibi SPECT.

A, From top to bottom row, representative frontal view of control mouse, 40 Gy PH, 40 Gy PHL, and 60 Gy PH RT mice 8 weeks post-RT. Red arrows highlight differences in apical left ventricular (LV) perfusion. **B,** Basal and apical LV tracer uptake at 8 weeks post-RT (n= 4 per group). *P<0.05, **P<0.01, (details in Supplementary Table S2).

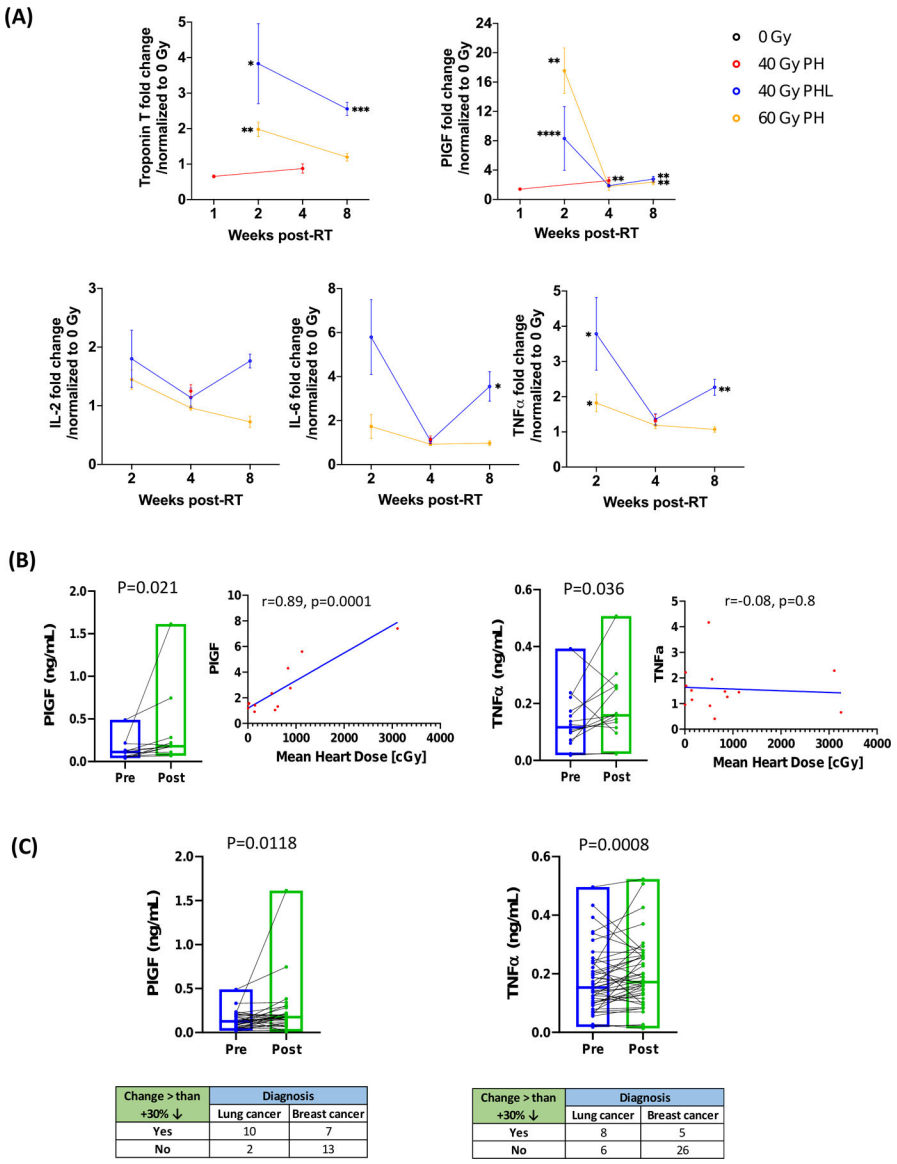

Change > than +30% ↓	Diagnosis	
	Lung cancer	Breast cancer
Yes	10	7
No	2	13

Change > than +30% ↓	Diagnosis	
	Lung cancer	Breast cancer
Yes	8	5
No	6	26

Figure 6. Biochemical analysis of irradiated mouse heart tissue segments and human plasma. **A,** Effects of focal cardiac RT on markers of cardiovascular injury and inflammation at 1, 2, 4, and 8 weeks post 40 Gy PH, 40 Gy PHL, and 60 Gy PH RT (n= 3 or 4 per group unless otherwise noted). P<0.05, **P<0.01, ***P<0.001 (details in Supplementary Table S3). Cardiac tissue levels of troponin I were above detection range of assay. **B,** Effects of thoracic RT in lung cancer patients on PlGF and TNFα and correlation of fold change in these markers with mean heart dose. **C,** Comparison of PlGF and TNFα changes in lung versus breast cancer patients. Data are from 14 lung cancer patients and 32 breast cancer patients. Missing data is due to undetectable marker levels in several plasma samples.